Applied Surface Science 270 (2013) 252–259

Contents lists available at SciVerse ScienceDirect

Applied Surface Science

journal homepage: www.elsevier.com/locate/apsusc

Electrodeposition of PdCu alloy and its application in methanol electro-oxidation

Ming-Wei Hsieh, Thou-Jen Whang*

Department of Chemistry, National Cheng Kung University, 1 University Road, Tainan 70101, Taiwan

ARTICLE INFO

Article history:
Received 6 November 2012
Received in revised form 3 January 2013
Accepted 4 January 2013
Available online 17 January 2013

Keywords:
Electrodeposition
PdCu alloy
Redox replacement
Methanol oxidation

ABSTRACT

This study demonstrates a simple electrodeposition method to fabricate the palladium–copper alloy on an ITO coated glass (PdCu/ITO) and its application in methanol electro-oxidation. Our approaches involve the co-reduction of Pd and Cu using triethanolamine (TEA) as a complexing agent in the electroplating bath and a Pd redox replacement of Cu on the surface of the as-prepared PdCu alloy. The phase structures, alloy compositions and morphologies of catalysts are determined by X-ray diffraction, energy dispersive spectrometer and scanning electron microscopy, respectively. X-ray diffraction shows that the particle size of PdCu deposits shrink when the alloy is deposited in a TEA-contained solution. The electrocatalytic properties of PdCu alloys and Pd redox replacement modified PdCu alloys for methanol oxidation have been investigated by cyclic voltammetry. The PdCu alloy with atomic ratio of 20.5% Cu exhibits higher catalytic activity toward methanol oxidation compared with a pure Pd catalyst. PdCu alloys with smaller particle sizes associated with TEA agent and the surface confined Pd replacement are found to have enhanced catalytic performance in the electro-oxidation of methanol.

1. Introduction

Direct methanol fuel cells (DMFCs) have received much attention for their applications in portable electronic devices and vehicles [1]. For the methanol oxidation reaction (MOR) in DMFC, Pt-based electrocatalysts are still indispensable and the most effective catalysts [2,3]. However, the high cost of Pt and its low catalytic activity for alcohol electro-oxidation in alkaline media are major obstacles for its wide applications [4–6]. As an alternative to the more expensive Pt, Pd shows great potential as an effective catalyst for formic acid [7–10] and alcohol oxidations in alkaline media [11–13].

In recent years, many binary and ternary metal compounds have been developed in the form of Pd alloys and Pd overlayer structures. These combinations such as PdRu, PdAu, PdAg and PdSn, etc. [7,9–12] have been reported, aiming at enhancing the electrocatalytic activity toward the oxidation of small organic molecules. Besides, nanoporous Pd structure formed through selectively removing Cu atoms on the surface of Pd alloy has improved catalytic performance in methanol oxidation [14]. Bertotii and co-workers reported that the anodic oxidation of alcohols are facilitated on Cu electrodes and further oxidized in alkaline media [15]. Furthermore, Cu has been reported to play an assistant role in enhancing the catalytic activity of Pd and Pt in alcohol oxidations [16–18]. Considering that Pd and Pt have similar catalytic properties, we used a simple electrodeposition method to combine Pd and Cu to generate intriguing catalytic activities in the electro-oxidation of methanol.

In this study, we fabricated a series of Pd–Cu alloys on indium tin oxide coated glasses (PdCu/ITO) via a constant-potential deposition of the two elements. According to previous reports, a complexing agent, triethanolamine (TEA) was found to suppress the growth of copper during the co-deposition with indium and selenium [19,20]. With an original intention to obtain a Pd-rich alloy by electrodeposition, we added TEA into the electroplating bath containing Pd^{2+} and Cu^{2+}. X-ray diffraction (XRD) and scanning electron microscopy (SEM) showed that the PdCu alloy we made has smaller particle sizes compared with those deposited in TEA-free solutions. Cyclic voltammetry (CV) showed that alloys deposited in TEA-involved solutions have higher hydrogen desorption areas, which means a higher electrochemical surface area (ECSA) of alloys were obtained.

Besides, in the system of Pd^{2+} and Cu^{2+} co-deposition, underpotential deposition (UPD) of Cu took place on the surface of Pd. This is compatible with the fact that UPD happens when an element with a small work function (φ_{Cu} = 4.5 eV) is deposited on a foreign metal with a relatively large work function (φ_{Pd} = 5.1 eV) [21]. Copper UPD in many alloy systems could be replaced by nobler metals in their corresponding solutions, which is commonly named as a redox replacement [22,23]. The positive difference between the standard reduction potential of Pd and Cu makes a redox replacement thermodynamically favorable and spontaneously happening.

* Corresponding author at: Department of Chemistry, National Cheng Kung University, 1 University Road, Tainan 70101, Taiwan. Tel.: +886 6 2757575 65356; fax: +886 6 2740552.
E-mail addresses: twhang@mail.ncku.edu.tw, z8108040@email.ncku.edu.tw (T.-J. Whang).

0169-4332/$ – see front matter © 2013 Elsevier B.V. All rights reserved.
http://dx.doi.org/10.1016/j.apsusc.2013.01.012

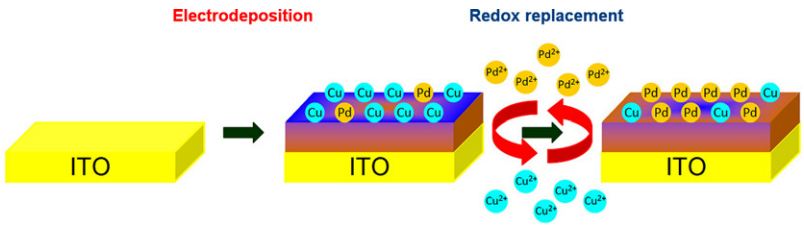

Fig. 1. Scheme describing the redox replacement of Cu atoms by Pd ions followed by the codeposition of PdCu thin film on ITO.

The combination of the two techniques of UPD and redox replacement provides a manipulable strategy for the surface modification of electrocatalysts. We used the beneficial of Cu UPD during the co-deposition of PdCu with the subsequent replacement by Pd to form a Pd modified PdCu alloy. Catalysts deposited in the presence of TEA and followed by a Pd redox replacement showed higher catalytic activities toward methanol oxidation.

2. Experimental

2.1. Preparation of PdCu and TEA–PdCu

All chemicals were used as received and prepared in deionized water. Briefly, 0.36 g $PdCl_2$ and 0.50 g $CuSO_4{\cdot}5H_2O$ were separately added with 3 mL HCl, followed by diluted to 8 mmol L^{-1} after their complete dissolution. A certain amount of crystalline boric acid (H_3BO_3) was added to the two solutions as a buffering agent (40 mmol L^{-1} in each bath). The pH values of $PdCl_2$ and $CuSO_4{\cdot}5H_2O$ solutions were ca. 2.30. Then 8 mmol L^{-1} Pd^{2+} was mixed with 8 mmol L^{-1} Cu^{2+} in various volumetric ratios of 1:0, 9:1, 4:1, 3:1 and 2:1. To compare the effect of a complexing agent, 0.024 mol L^{-1} TEA is added into each of the mixed-ion solution. However, the pH values of electroplating solutions greatly increased after TEA was added. Their pH values were adjusted to 2.30 by adding drops of dilute HCl before the experiment. In each deposition, 6 mL of the mixed-ion solution was injected into a quartz vessel. The electrodeposition and electrochemical measurements were conducted in a three-electrode cell using a CH Instrument 627C workstation. The working electrode was a 1.0 cm × 3.0 cm ITO glass. The counter electrode was a 1.0 cm × 3.0 cm platinum sheet and the reference electrode was Ag/AgCl.

PdCu bimetallic alloys with different Pd/Cu ratios were prepared by constant-potential deposition. The mechanism of electrodeposition of Pd and Cu from their mixed-ion solutions has been reported elsewhere [24]. In this work, the applied potential was −0.4 V vs. Ag/AgCl, which was the most suitable potential for depositing PdCu alloy on an ITO glass according to previous experiences [16]. Each deposition was completed until the electric charge accumulated to 1.2 C. The obtained sample was denoted as Pd_xCu_y where x to y stands for the molar ratio of Pd^{2+} to Cu^{2+} in the electroplating bath. For comparison, alloys from solutions containing TEA were denoted as TEA–Pd_xCu_y.

2.2. Preparation of Pd/TEA–PdCu

After the electrodeposition, the as-prepared TEA–PdCu was immersed in an 8 mmol L^{-1} $PdCl_2$ solution under an open circuit potential (OCP) for 600 s. Because the equilibrium potential of Pd^{2+}/Pd is higher than that of Cu^{2+}/Cu, Pd^{2+} was reduced by Cu and metallic Pd was deposited on the original sites of Cu through a redox replacement [14,23]. Fig. 1 shows a schematic representation of Cu replaced by Pd on the surface of TEA–PdCu. After replacement with Pd, the new PdCu electrode was denoted as Pd/TEA–Pd_xCu_y.

2.3. Characterization

Crystalline structures of PdCu electrodeposits were studied by a powder X-ray diffraction (XRD, Shimadzu XRD-6100 diffractometer) using the Cu Kα radiation (0.154056 Å). The diffraction angle (in 2θ) was collected at a scanning rate of 1° per minute with a step of 0.02°. Surface morphology of the alloy was characterized by a scanning electron microscopy (SEM, Hitachi S-4100) equipped with an energy dispersive spectroscope (EDS). All experiments were carried out at ambient temperatures.

3. Results and discussion

3.1. Physical characterization of the electroplating bath and PdCu films

The electrochemical behaviors of Pd and Cu ions on an ITO substrate are investigated by CV. Fig. 2 shows a collection of CV plots in which the Pd^{2+}/Cu^{2+} molar ratio is 1:0, 9:1, 4:1 and 3:1, respectively. There are two apparent cathodic peaks (c_1, c_2) and anodic peaks (a_1, a_2) in the forward scan and reverse scan, respectively. Those peaks are owing to the reduction and oxidation processes related to Pd. As observed, Pd is reductively deposited at ca. +0.1 V (c_1). The cathodic peak c_2 at −0.4 V is due to the formation of PdH_x followed by a steep current increase as a result of hydrogen evolution at the negative end of the potential. On the return scan, a_2 is the peak of hydrogen desorption from the substrate at a potential of 0.0 V. Finally, the scan encountered the oxidation peak a_1 which arose from the dissolution of Pd. The current densities of c_1/a_1 and c_2/a_2 couples reduce with the decrease in Pd^{2+} concentration. In general, CV behaviors of the species on an ITO substrate are similar to those reported on a glassy carbon electrode [25]. However, the oxidation and reduction peaks related to Cu are less obvious in these diagrams. Cathodic peaks for the reduction of Cu^{2+} are not clearly showed in these CVs, but a slight increase of anodic peak at

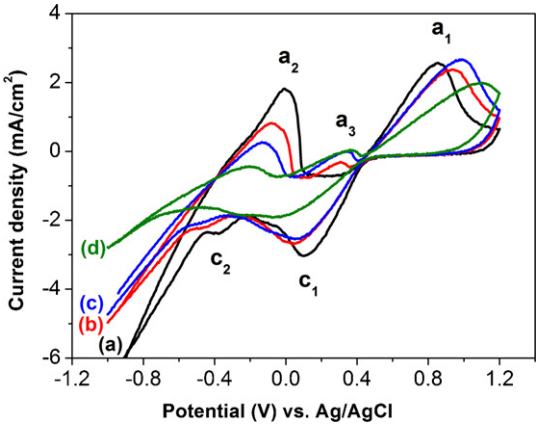

Fig. 2. CV plots of Pd^{2+} plus Cu^{2+} in the molar ratio of (a) 1:0, (b) 9:1, (c) 4:1 and (d) 3:1 in a 0.04 mol L^{-1} H_3BO_4 solution.

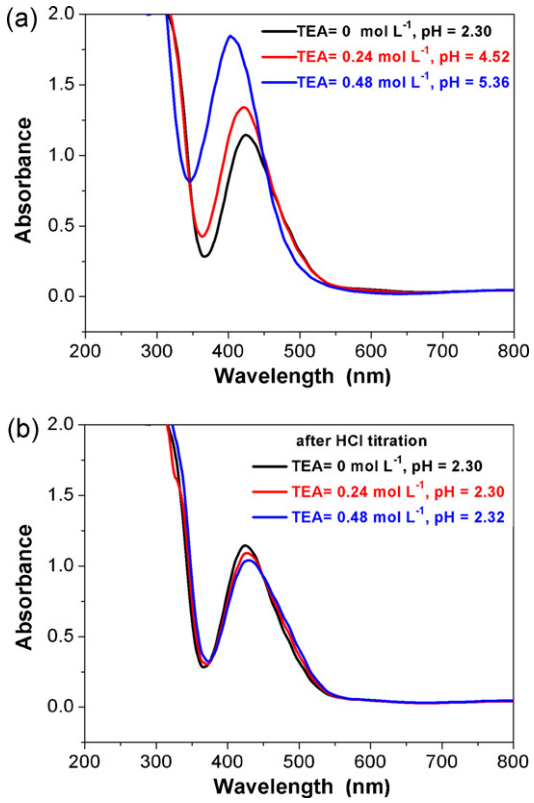

Fig. 3. UV–vis absorption spectra of the mixed solution of Pd^{2+} and Cu^{2+} in the molar ratio of 2:1 with different concentrations of TEA: (a) without HCl and (b) with HCl adjustment to pH 2.30.

+0.3 V is observed as Cu^{2+} content increases, which signifies that it is connected to the oxidation of Cu^{2+} species.

To investigate the effect of TEA in the electroplating solution, UV–vis spectra of Pd^{2+} plus Cu^{2+} in the molar ratio of 2:1 with different amount of TEA are investigated. In Fig. 3, the absorption peak appears at 425 nm is attributed to the ligand to metal charge transfer band of $[PdCl_4]^{2-}$ species [26]. When TEA is added, pH values of the electroplating baths increase and their absorption peaks blue shift (Fig. 3a). In order to make the plating bath suitable for the electrodeposition of Pd, dilute HCl is added to adjust the pH value to 2.30 (the same pH as the TEA-free solution). Fig. 3b shows that the absorption shifts are canceled with a slight decrease in absorbance after their pH values are adjusted. According to these observations, the electroplating baths have an unchanged Pd^{2+} to Cu^{2+} ratio after their addition of TEA and dilute HCl titration. However, CV plots show different electrochemical behaviors for the bath with different concentrations of TEA (Fig. 4). The potentials for Pd and Cu reduction (c_1 and c_3) are distinctly separable when there is no complexing agent. For the constant-potential deposition of two species at a time, an overlap of their cathodic peaks is expected. As seen in figure, the two peaks seem to merge with each other when the amount TEA increased to 0.24 and 0.48 mol L^{-1}, thus providing a narrow deposition window for the co-reduction of Pd^{2+} and Cu^{2+}.

It is feasible to prepare noble metal monolayers on the surface of PdCu alloy based on the redox replacement of UPD Cu layer in a solution containing nobler metal ions. This provides a simple pathway for designing a novel electrocatalyst with monolayers of metal such as Pt and Pd. In this work, we chose Pd as the metal for replacement. Before the replacement reaction commenced, we ascertained the occurrence of UPD Cu on Pd substrates by CV experiments. Fig. 5 is the comparison of CV plots between an ITO electrode and a Pd coated ITO electrode in the solution containing 8 mmol L^{-1}

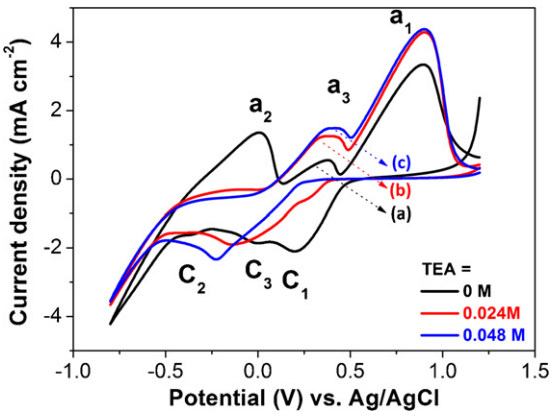

Fig. 4. CV plots of Pd^{2+}/Cu^{2+} in the molar ratio of 2:1 with (a) 0, (b) 0.24 and (c) 0.48 mol L^{-1} TEA.

$CuSO_4$. Interestingly, the CV plot of Pd/ITO showed three different behaviors from that of a pure ITO glass. First, the potential for the bulk deposition of Cu shifts to more positive values (as showed by dashed line), which means the deposition of Cu is much easier to occur on a Pd/ITO electrode. Second, the small reduction peak at the potentials more positive than the bulk deposition potential is associated with the formation of the Cu UPD layers on the Pd surface. The last one is that the cathodic peak for Cu oxidation shifts from 0.30 V to 0.45 V, showing Cu atoms oxidized less easily on a Pd/ITO electrode than on an ITO substrate. According the above observations, PdCu alloy would be produced and followed by the underpotential deposition of Cu on the surface of Pd when Pd^{2+} and Cu^{2+} are deposited simultaneously. When a PdCu-modified ITO electrode was immersed into an aqueous solution of 8 mmol L^{-1} $PdCl_2$, the redox replacement of UPD Cu with Pd, driven by the large gap of standard reduction potentials between Cu^{2+}/Cu and Pd^{2+}/Pd, yielded new Pd layers on the PdCu surface.

Fig. 6 shows the XRD pattern of each alloy. Standard diffractions of Pd are marked by yellow dashed line. The four peaks at 40.1, 46.7, 68.1 and 82.1° are characteristic of diffractions from the face-centered cubic (fcc) system corresponding to the (1 1 1), (2 0 0), (2 2 0) and (3 1 1) planes, respectively. For PdCu alloys, the diffraction peaks locate between the projected 2θ values for pure Pd and Cu, which indicates the formation of a single-phase uniform fcc PdCu alloy. By comparison with pure Pd, the diffraction peaks of PdCu alloys shifted to higher angles with an increase in Cu content because of the substitution of smaller Cu atoms for Pd atoms. The

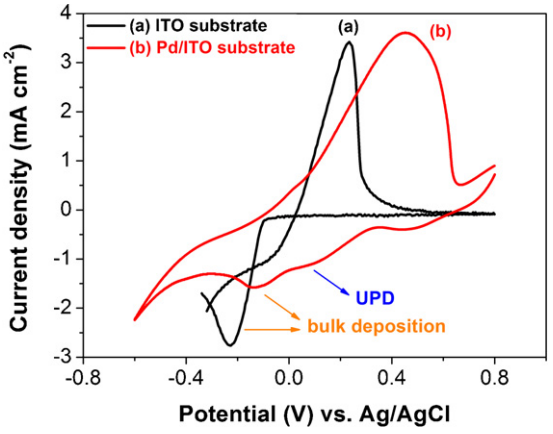

Fig. 5. CVs for 8 mmol L^{-1} $CuSO_4$ in 0.04 mol L^{-1} H_3BO_4 with (a) ITO and (b) Pd coated ITO electrode (Pd/ITO). The scan rate was 25 mV s^{-1}.

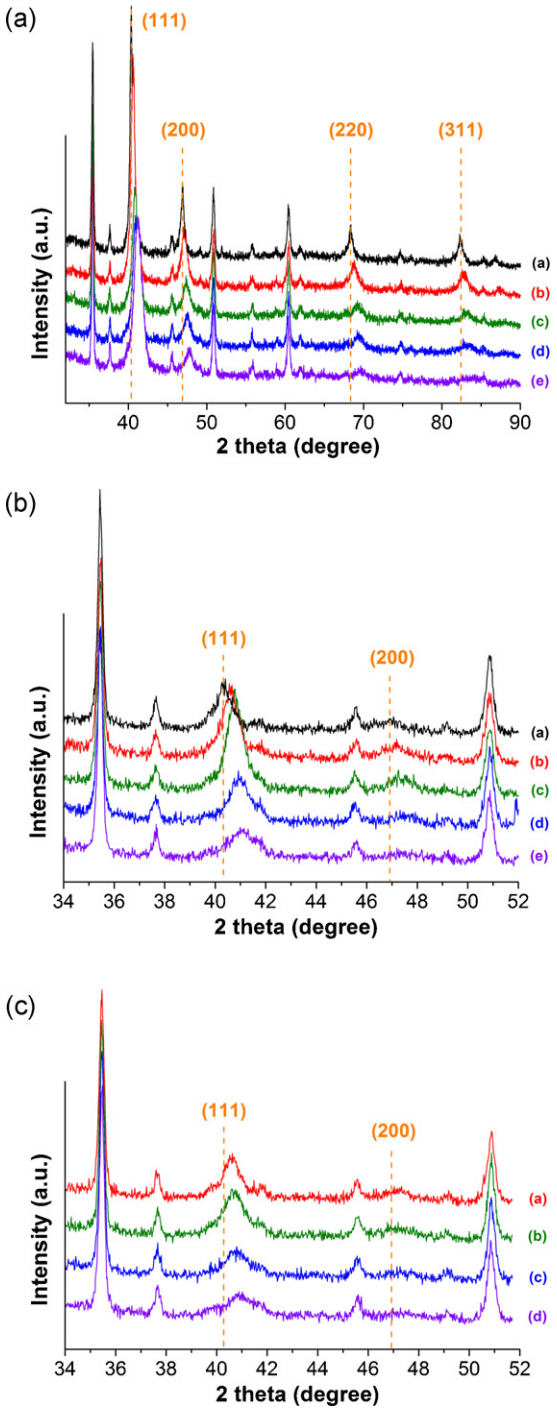

Fig. 6. XRD patterns of (a) PdCu, (b) TEA–PdCu and (c) Pd/TEA–PdCu alloys. The standard diffractions of pure Pd are marked by dashed lines.

average particle size (d) is estimated using the Scherrer's formula [27] based on the (1 1 1) peak:

$$d = \frac{0.941\lambda}{\beta \cos\theta} \quad (1)$$

where λ is the wavelength of X-ray, β is the full width at half maximum (FWHM) of (1 1 1) peak (in radian), and θ is the diffraction angle at Pd (1 1 1) crystal facet (in degree). The average crystalline sizes of PdCu and the calculated lattice constants are given in Tables 1 and 2. The average particle size decreases from 26.6 to 7.1 nm with increasing the Cu nominal fraction (fraction in Pd^{2+} plus Cu^{2+} mixed solution) from 0 to 33.4% in the PdCu

Table 1
Derived structural information for PdCu alloys.

Pd^{2+}:Cu^{2+} ratio in the solution	$2\theta_{(1\,1\,1)}$ (°)	a_{fcc} (nm)	Cu_{alloy} (%)	Size (nm)
1:0	40.36	0.3868	–	25.7
9:1	40.59	0.3847	15.73	14.4
4:1	40.87	0.3821	25.01	10.4
3:1	40.91	0.3818	26.31	10.1
2:1	41.25	0.3788	37.11	7.2

composition. It should be noted that particle sizes of PdCu deposits become smaller in the presence of TEA, as suggested by their larger FWHM. Fig. 6c shows the XRD patterns of Pd decorated PdCu alloys, in which the (1 1 1) peak exhibits slightly skewed to small angles (Table 2), signifying an increase in Pd content. There is a dependence of the Pd lattice constant on the atomic fraction of Cu. It is apparent that the lattice constant of Pd (a_{Pd}) for all the PdCu catalysts shrinks and decreases with increasing the Cu content. This is reasonably explained by the solid solution formation between Pd atoms (covalent radius of 0.139 nm) and smaller Cu atoms (covalent radius of 0.132 nm). The Pd atomic ratios in the bimetallic PdCu alloys are calculated quantitatively from the difference between the measured lattice constants and determined via Vegard's law [28], using the following two equations:

$$1/d^2_{(hkl)} = \frac{(h^2 + k^2 + l^2)}{a^2} \quad (2)$$

$$a_{PdCu} = a_{Cu}x_{Cu} + (1 - x_{Cu})a_{Pd} \quad (3)$$

where $d_{(hkl)}$ is the interplanar spacing, a is the lattice constant and x is the molar fraction.

The composition of each alloy was examined according to its corresponding EDS result and was referenced to the calculated value by its lattice constant. The EDS examined Cu atomic ratio for each alloy is shown in Table 3. We can observe that the Pd content increases with the addition of TEA in the bath. This is compatible with the fact that TEA was reported to suppress the reduction of Cu ions in solution during the co-deposition [19,20,29]. Moreover, each value of Cu content in Table 3 is lower than the respective value estimated by Vegard's law (Cu_{alloy} in Tables 1 and 2). This phenomenon was suggested by the fact that the EDS analysis is less sensitive to the relatively light Cu atom in the PdCu alloy. However, the relationship between Pd fractions in solutions and their atomic ratios in different alloys is quite linear according to both EDS results and XRD calculations (Fig. 7).

Fig. 8 is the SEM images of PdCu alloys without TEA. As shown in this micrograph, the surface morphology of the electrocatalysts is strongly dependent on the plating bath composition. In Fig. 8a, the

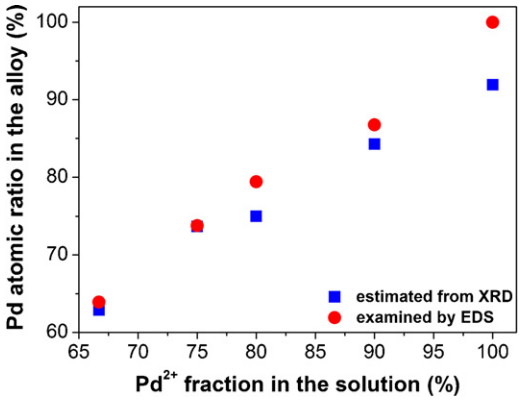

Fig. 7. Plot for comparison of the calculated Pd contents and EDS examined results in PdCu alloys.

Table 2
Derived structural information for TEA–PdCu and Pd/TEA–PdCu alloys.

Pd^{2+}:Cu^{2+} ratio in the solution	TEA–PdCu				Pd/TEA –PdCu			
	$2\theta_{(111)}$ (°)	a_{fcc} (nm)	Cu_{alloy} (%)	Size (nm)	$2\theta_{(111)}$ (°)	a_{fcc} (nm)	Cu_{alloy} (%)	Size (nm)
1:0	40.38	0.3867	–	11.1	–	–	–	–
9:1	40.58	0.3848	15.40	11.5	40.59	0.3847	15.73	10.3
4:1	40.78	0.3830	21.91	11.1	40.65	0.3841	17.87	7.6
3:1	40.93	0.3816	26.74	8.5	40.72	0.3835	19.98	7.1
2:1	41.08	0.3802	31.82	6.2	40.95	0.3815	27.42	4.1

Table 3
EDS estimated Cu atomic ratios of the electrocatalysts.

Cu fraction in the mixed solution (%)	Cu atomic ratio in PdCu sample (%)	Cu atomic ratio in TEA–PdCu sample (%)	Cu atomic ratio in Pd/TEA–PdCu sample (%)
0	0	0	–
10	13.25	11.31	11.86
20	20.59	20.80	17.75
25	26.21	26.35	18.45
33.3	36.09	27.24	23.29

Pd deposit appears as dendrimer structures. In Fig. 8b–d, however, the surface becomes composed of many smaller rhomboids with the involvement of Cu atoms into Pd skeletons. Fig. 9a and b shows the micrographs of Pd_4Cu_1 and Pd_2Cu_1 films with TEA. Compared with SEM images of PdCu samples obtained in TEA-free plating baths, PdCu deposits appear to be compact and granulated. The granules are nearly spherical in shape rather than rhomboid. Metal films after Pd redox replacement have similar spherical microstructures (Fig. 9c and d).

3.2. Electrochemical property of the electrocatalysts and activity toward MOR

Electrocatalytic activities of PdCu catalysts for methanol oxidation were analyzed by CV in a 1.0 mol L^{-1} methanol solution containing 1.0 mol L^{-1} KOH. Fig. 10 compares the overall CVs of PdCu electrocatalysts in which there are various Pd to Cu ratios. The methanol oxidation behavior is characterized by two well defined anodic current peaks: one in the forward and the other one in the reverse scan. In the forward scan, the anodic peak is corresponding to the oxidation of freshly chemisorbed methanol species and its magnitude is proportional to the amount of methanol oxidized. The anodic peak in the reverse scan is associated with the removal of carbonaceous species not completely oxidized in the forward scan [30,31]. The mechanism for methanol oxidation in basic media at Pd electrodes has been reported earlier [32]:

$$Pd{-}CH_3OH + OH^- \rightarrow Pd{-}CH_3O + H_2O + e^- \quad (4)$$

$$Pd{-}CH_3O + OH^- \rightarrow Pd{-}CH_2O + H_2O + e^- \quad (5)$$

$$Pd{-}CH_2O + OH^- \rightarrow Pd{-}CHO + H_2O + e^- \quad (6)$$

$$Pd{-}CHO + OH^- \rightarrow Pd{-}CO + H_2O + e^- \quad (7)$$

According to the mechanism, Pd surface will finally be poisoned by CO species, which will reduce the catalytic activity toward MOR. In alkaline solutions, additional surface chemical reactions are

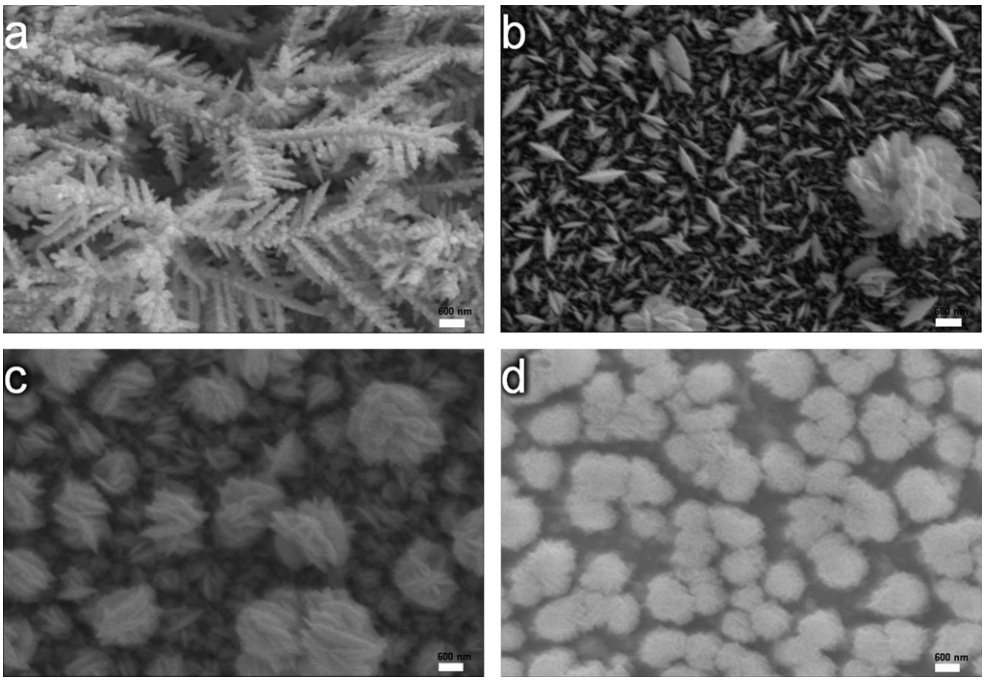

Fig. 8. SEM of PdCu alloys prepared from the deposition of Pd^{2+}/Cu^{2+} in the molar ratio of (a) 1:0, (b) 4:1, (c) 3:1 and (d) 2:1.

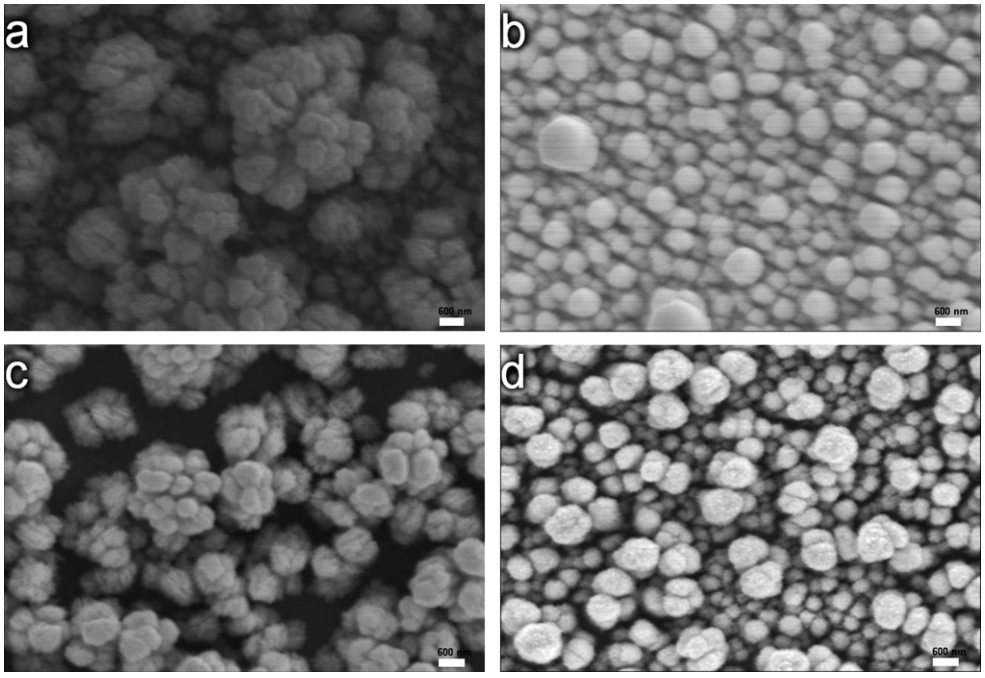

Fig. 9. SEM of PdCu alloys prepared from TEA-contained solution in which Pd^{2+} to Cu^{2+} molar ratios is (a) 4:1 and (b) 2:1. (c) and (d) refer to the films after Pd replacement modification of (a) and (b), respectively.

possible, which can be used to remove surface-adsorbed species from the Pd metal and regenerate the Pd metal [32]. The CV curves shown in Fig. 10 were analyzed by the current density peaks (j_p) and current peak potentials (E_p) for the forward-scan peak and their values are shown in Table 4.

For those catalysts deposited from TEA-free solutions, PdCu alloys show higher current densities toward MOR than that of pure Pd, signifying the catalytic activities are enhanced due to the incorporation of Cu. The optimal Cu atomic ratio among the PdCu alloys is 20.59% according to the EDS analysis. For alloys deposited in the presence of TEA, all the oxidation peaks increase compared with their TEA-free counterparts. TEA–Pd_4Cu_1 shows the highest current density of 21.04 mA cm^{-2}. Alloys deposited with TEA and followed by Pd redox replacement show the greatest oxidation peak in these three categories. Pd/TEA–Pd_4Cu_1 in which the Cu atomic ratio is 17.75% exhibits the highest current density, 29.00 mA cm^{-2} in our samples (Fig. 10c).

To explain the increase of current density in methanol electro-oxidation, we compare the cyclic voltammograms of Pd_4Cu_1 alloys in a 0.1 mol L^{-1} $HClO_4$ solution. The CV demonstrates three potential regions typical of Pt group metals: the hydrogen adsorption/desorption region (H_{ads}/H_{des}) in −0.30 to 0.15 V, the double layer region in 0.15 to 0.50 V and the oxide formation region above 0.50 V. As observed, all Pd-based catalysts show characteristic peaks of oxidation at ~0.60 V in the forward scan and reduction peaks of Pd oxides at ~0.40 V in the reverse scan. Compared with Pd, each of PdCu alloy shows a new anodic peak at 0.20–0.40 V, which is due to the leaching of exposed Cu atoms in the alloy surface [33]. Theoretically, the electrochemical active surface area (ECSA) of those Pd-containing catalysts cannot be measured based on the hydrogen adsorption/desorption, because we cannot separate H_{ads} and H_{abs} in the α phase of PdH_x [34]. However, we find the alloys deposited in TEA-contained solutions show a shoulder (0.0–0.1 V) within the H_2 desorption peak. The alloy after a Pd redox replacement process shows the largest H_2 desorption area among the three samples in the CV diagrams. Overall, the H-desorption areas of PdCu alloys follow the order: Pd/TEA–Pd_4Cu_1 > TEA–Pd_4Cu_1 > Pd_4Cu_1, which is consistent with the order of current densities in methanol oxidations. TEA in our study plays a role in suppressing the growth of Cu atoms. The enhanced catalytic abilities of TEA–PdCu alloys may result from the combination effects of particle size shrinkages, the alteration in surface morphologies, and the increase in Pd/Cu ratios, as can be seen in Figs. 6 and 9 and Table 3, respectively. These elements enhance the surface active areas of PdCu alloys, which in turn improve the catalytic performance of electrocatalysts in methanol oxidation.

Fig. 11.

It has been reported that the alloying with Cu atoms would produce an electronic modification of Pd layers by strain and alloying effects [35–37], which may provide unique surface sites for methanol adsorption and subsequent electro-oxidation. The enhanced methanol oxidation activity also supports that the

Table 4
Peak potential (E_p) and peak current density (j_p) results from the CVs of methanol oxidation.

Pd^{2+}:Cu^{2+} ratio in the solution	PdCu		TEA–PdCu		Pd/TEA–PdCu	
	E_p (V)	j_p (mAcm^{-2})	E_p (V)	j_p (mAcm^{-2})	E_p (V)	j_p (mAcm^{-2})
1:0	0.05	6.91	0.08	13.18	–	–
9:1	-0.02	7.85	0.13	16.08	0.17	17.53
4:1	0.02	11.81	0.14	21.04	0.26	29.00
3:1	0.03	9.52	0.16	18.32	0.22	24.08
2:1	0.04	7.11	0.07	13.35	0.12	15.85

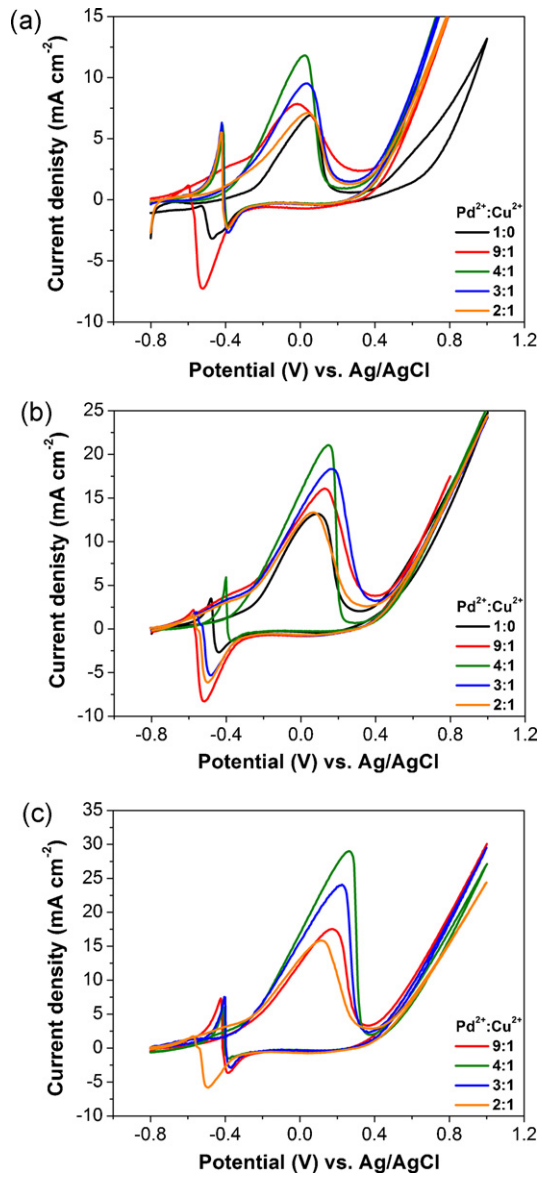

Fig. 10. CVs of (a) PdCu, (b) TEA–PdCu and (c) Pd/TEA–PdCu alloys in 1.0 mol L^{-1} methanol with 1.0 mol L^{-1} KOH. The scan rate was 25 mV s^{-1}.

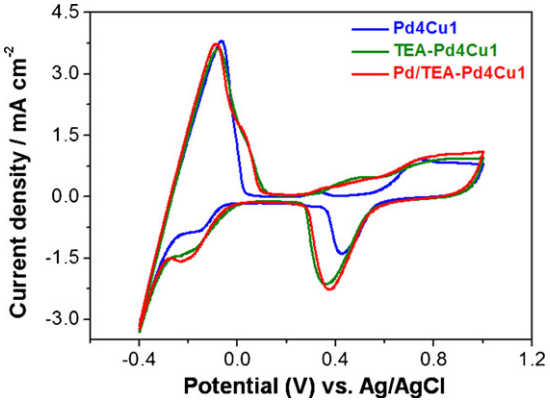

Fig. 11. CVs of Pd_4Cu_1, TEA–Pd_4Cu_1 and Pd/TEA–Pd_4Cu_1 in a 0.1 mol L^{-1} $HClO_4$ solution. The scan rate was 10 mV s^{-1}.

particle surface in rich in Pd when the alloy is deposited in a TEA-contained bath, as the presence of Cu on Pd would block the active sites [38].

The density functional theory (DFT), which predicts the center of d-band energy (ε_d) of a metal catalyst, has been used to interpret the effects of the second metal. Hammer and Nørskov [39] have corroborated the position of ε_d plays a governing role in determining the affinity of transition metals toward a variety of adsorbates such as O, CO, H, etc. The higher this center locates with respect to the Fermi level, the stronger is the interaction of the metal with adsorbates. Fouda-Onana and Savadogo [40] have reported that the d-band center of Pd shifts to a lower value after the incorporation of Cu atoms. The change of ε_d can influence their catalytic reaction kinetics by altering the adsorption energies of reaction intermediates. When the Pd content reaches 75% atomic ratio, the d-band center shifts to −2.798 eV. Thus, the lower value of d-band center for PdCu with 25% Cu content may result in its higher electrocatalytic activity. In our experimental results, PdCu samples with an average of 20% Cu atomic ratio show the highest catalytic activity toward methanol oxidation.

4. Conclusion

In this work, we enhance the catalytic ability of PdCu alloys toward methanol oxidation by adding a complexing agent of TEA. The TEA-contained Pd^{2+} plus Cu^{2+} mixed solutions produce alloys with smaller particle sizes, as evidenced by XRD results. By taking advantages of the UPD phenomenon during co-deposition of PdCu and the following Pd redox replacement, we further modify the surface of TEA–PdCu alloys. Electrochemical measurements show that Pd incorporated with Cu atoms has enhanced electrocatalytic activity toward methanol oxidation. This enhancement is probably due to a good synergistic effect between Cu and Pd. In particular, the bimetallic PdCu catalyst with a composition of ca. 20.5% Cu content exhibits the highest catalytic capability for methanol oxidation. The fabrication of PdCu alloys via electrodeposition is simple and helpful for the development of effective catalysts suitable for direct methanol fuel cells.

Acknowledgement

This work was partially supported by the National Science Council of the Republic of China, Taiwan (NSC 101-2113-M-006-003).

References

[1] S. Basri, S.K. Kamarudin, W.R.W. Daud, Z. Yaakub, International Journal of Hydrogen Energy 35 (2010) 7957–7970.
[2] L.H. Jiang, G.Q. Sun, X.S. Zhao, Z.H. Zhou, S.Y. Yan, S.H. Tang, G.X. Wang, B. Zhou, Q. Xin, Electrochimica Acta 50 (2005) 2371–2376.
[3] R. Chetty, S. Kundu, W. Xia, M. Bron, W. Schuhmann, V. Chirila, W. Brandl, T. Reinecke, M. Muhler, Electrochimica Acta 54 (2009) 4208–4215.
[4] H.S. Liu, C.J. Song, L. Zhang, J.J. Zhang, H.J. Wang, D.P. Wilkinson, Journal of Power Sources 155 (2006) 95–110.
[5] Z.D. Wei, S.H. Chan, Journal of Electroanalytical Chemistry 569 (2004) 23–33.
[6] M. Rosenbaum, U. Schröder, F. Scholz, Journal of Solid State Electrochemistry 10 (2006) 872–878.
[7] Z.L. Liu, X.H. Zhang, S.W. Tay, Journal of Solid State Electrochemistry 16 (2012) 545–550.
[8] N.C. Cheng, H.F. Lv, W. Wang, S.C. Mu, M. Pan, F. Marken, Journal of Power Sources 195 (2010) 7246–7249.
[9] Y. Suo, I.M. Hsing, Electrochimica Acta 56 (2011) 2174–2183.
[10] L. Dai, S.Z. Zou, Journal of Power Sources 196 (2011) 9369–9372.
[11] M.L. Wang, W.W. Liu, C.D. Huang, International Journal of Hydrogen Energy 34 (2009) 2758–2764.
[12] W. Du, K.E. Mackenzie, D.F. Milano, N.A. Deskins, D. Su, X. Teng, ACS Catalysis 2 (2012) 287–297.
[13] G.L. Li, L.H. Jiang, Q.A. Jiang, S.L. Wang, G.Q. Sun, Electrochimica Acta 56 (2011) 7703–7711.
[14] C. Xu, Y. Liu, J. Wang, H. Geng, H. Qiu, Journal of Power Sources 199 (2012) 124–131.

[15] T.R.L.C. Paixão, E.A. Ponzio, R.M. Torresi, M. Bertotti, Journal of the Brazilian Chemical Society 17 (2006) 374–381.
[16] L.S. Jou, J.K. Chang, T.J. Whang, I.W. Sun, Journal of the Electrochemical Society 156 (2009) D193–D197.
[17] R.F. Wang, B.X. Wei, H. Wang, S. Ji, J.L. Key, X.T. Zhang, Z.Q. Lei, Ionics 17 (2011) 595–601.
[18] C.X. Xu, Y.Q. Liu, J.P. Wang, H.R. Geng, H.J. Qiu, ACS Applied Materials & Interfaces 3 (2011) 4626–4632.
[19] C.J. Huang, T.H. Meen, M.Y. Lai, W.R. Chen, Solar Energy Materials and Solar Cells 82 (2004) 553–565.
[20] K. Kondo, N. Ishida, J. Ishihawa, T. Matsubara, Journal of the Electrochemical Society 138 (1991) 3629–3633.
[21] D.M. Kolb, M. Przasnyski, H. Gerischer, Journal of Electroanalytical Chemistry 54 (1974) 25–38.
[22] J. Zhang, K. Sasaki, E. Sutter, R.R. Adzic, Science 315 (2007) 220–222.
[23] S.R. Brankovic, J.X. Wang, R.R. Adzic, Surface Science 474 (2001) L173–L179.
[24] D. Reyter, D. Belanger, L. Roue, Journal of Physical Chemistry C 113 (2009) 290–297.
[25] T.R. Soreta, J. Strutwolf, C.K. O'Sullivan, Langmuir 23 (2007) 10823–10830.
[26] T. Teranichi, M. Miyake, Chemistry of Materials 10 (1998) 594–600.
[27] J.I. Langford, A.J.C. Wilson, Journal of Applied Crystallography 11 (1978) 102–113.
[28] A.R. Denton, N.W. Ashcroft, Physical Review A 43 (1991) 3161–3164.
[29] R.N. Bhattacharya, A.M. Fernandez, Solar Energy Materials 76 (2003) 331–337.
[30] J.C. Huang, Z.L. Liu, C.B. He, L.M. Gan, Journal of Physical Chemistry B 109 (2005) 16644–16649.
[31] O. Savadogo, K. Lee, K. Oishi, S. Mitsushima, N. Kamiya, K.I. Ota, Electrochemistry Communications 6 (2004) 105–109.
[32] B. Tao, J. Zhang, S. Hui, X. Chen, L. Wan, Electrochimica Acta 55 (2010) 5019–5023.
[33] C.X. Xu, H.Y. Ma, Y. Ding, Chemistry of Materials 21 (2009) 3110–3116.
[34] S. Trasatti, O.A. Petrii, Journal of Electroanalytical Chemistry 327 (1992) 353–376.
[35] J.R. Kitchin, J.K. Nørskov, M.A. Barteau, J.G. Chen, Journal of Chemical Physics 120 (2004) 10240–10246.
[36] A. Ruban, B. Hammer, P. Stoltze, H.L. Skriver, J.K. Nørskov, Journal of Molecular Catalysis A 115 (1997) 421–429.
[37] V.R. Stamenkovic, B.S. Mun, P.N. Ross, K.J.J. Mayrhofer, N.M. Markovic, Journal of the American Chemical Society 128 (2006) 8813–8819.
[38] K. Brandt, M. Steinhausen, K. Wandelt, Journal of Electroanalytical Chemistry 616 (2008) 27–37.
[39] B. Hammer, J.K. Nørskov, Surface Science 343 (1995) 211–220.
[40] F. Fouda-Onana, O. Savadogo, Electrochimica Acta 54 (2009) 1769–1776.